S. Hager, A. Bachmann, T. Hofmann, R. Engelbrecht and K. Glas

$CaCO_3$ deposits in reverse osmosis Part I – Shortcomings of current approaches leading to a new prediction model and monitoring device

Reverse osmosis (RO) is a widely used technology for providing brewing and process water in the beverage industry. In order to design the membrane process in a resource-saving and cost-effective way, the prediction of salt deposits in the membrane modules is of great importance. Since calcium and carbonate containing waters are very common, the solubility of $CaCO_3$ is often the limiting factor of the raw water yield. The prediction and thus the plant design is largely based on chemical saturation indices as the *LSI* and *S&DSI*. However, the calculation of these parameters is done on the basis of simplifications of the water chemistry, which are no longer necessary due to computer-aided calculation methods. Furthermore, there is no valid theory on $CaCO_3$ crystallisation based on fundamental energetic considerations. The classical crystallisation theory, which had been considered valid for decades, has proven to be insufficient. Improved theories are currently under discussion and a validation for $CaCO_3$ crystallisation is not available today. Nevertheless, the polymorphism of $CaCO_3$ seems to be of great value for the description of different saturation and crystallisation zones. Besides the most stable $CaCO_3$ form, calcite, the monohydrate calcium carbonate (MCC) has been characterised as crucial for the description of metastable solutions. Thus, the solubility product of calcite does not provide a suitable basis for predicting $CaCO_3$ precipitation as applied in the *LSI* and *S&DSI*. With this work, we introduce a hydrochemical simulation model of the RO process that can be linked to the chemical equilibria of other crystal forms of $CaCO_3$ such as the MCC. The calculations can be executed in the freely available water chemistry software PHREEQC. Besides the prediction of salt deposits, the literature shows a great need for reliable technical monitoring of fouling and especially inorganic fouling (scaling). In this context, we present a new fibre-optic based fouling detection system. Our proposed minimally invasive measurement technique allows spatially resolved measurements in membrane systems. The detection is based on the interaction of light and deposits such as salt on an optical fibre. The fibre optic sensor has the potential to provide the necessary database for validation and further improvement of the simulative prediction.

Descriptors: brewing water, process water, membrane, reverse osmosis, scaling, salt saturation, LSI, $CaCO_3$, fouling detection

1 Introduction

Water with a defined chemical composition is essential in numerous industries. Reverse osmosis (RO) is an effective, reliable and economical water treatment technology capable of meeting this demand. It is widely applied in the food technology industry, for example, for the preparation of brewing and process water. However, due to various factors, RO membranes often last only a limited time. Blockage of membranes, through either fouling or scaling, is a major factor which can reduce the financial feasibility of an RO plant [1]. For the production of brewing water often, tap water or well water is purified. The salt content of such waters is usually low, which is why low-pressure membranes can be applied. These membranes allow for high permeate water flux with acceptable salt rejection rates. As salt concentrations rise during the membrane desalination process, an oversaturation of salts has to be expected in the retentate stream. Especially the saturation state of $CaCO_3$ has to be considered since many groundwaters contain substantial amounts of calcium and carbonates [2]. Calcium carbonate is presumed to be the most widespread deposit in water systems [3]. However, for the design of low-pressure reverse osmosis systems, the main limiting factor is the feed water recovery rate, which in turn is limited by the supersaturation of salts and the risk of scaling. Usually a feed water recovery of 75 to 85 % is found in low-pressure applications. The higher the brine disposal

https://doi.org/10.23763/BrSc21-12hager

Authors

Simon Hager, Thomas Hofmann, Karl Glas, Water Systems Engineering, Chair of Food Chemistry and Molecular Sensory Science, TUM School of Life Sciences, Technische Universität München, Freising, Germany; Alexander Bachmann, Rainer Engelbrecht, Polymer Optical Fiber Application Center (POF AC), Technische Hochschule Nürnberg Georg Simon Ohm, Nuremberg, Germany; corresponding author: simon.hager@tum.de

costs, the higher the recovery required for a cost-efficient operation [4]. To meet this demand commonly chemicals are dosed for the stabilisation of oversaturated salts and a prevention of scaling. However, such chemicals can pollute the aquatic environment. Ecotoxicological investigations showed significant increased mortality rates for model organisms in contact to dilute reverse osmosis concentrates with anti-scalants [5]. In addition, also the permeate stream and thus the brewing water can be contaminated with an organic micro-pollutant, which originates from the anti-scalant. Initially, minor damages of membranes were held responsible for such a contamination of the permeate stream [6]. Today it is seems clear that even with intact membranes no sufficient rejection of anti-scalants or degradation products can be expected [7]. Avoiding the use of an anti-scalant, on the other hand, can lead to scaling, increased cleaning effort, accelerated membrane ageing and plant downtime [8, 9]. Considering these conflicting requirements, an accurate prognosis of salt precipitation seems important for future RO applications. Another way of approaching this challenge is to have reliable and practicable scaling monitoring techniques. Today's monitoring of especially early stage scaling is proving difficult and error prone. Neither current scaling detection systems nor prediction models provide sufficient results [10, 11]. For a needs-based dosage of salt-stabilising chemicals or the triggering of cleaning cycles a reliable prognosis or monitoring of the scaling state could be of great help.

The overall objective of this work is to overcome the technical-economic and environmental problems in the operation of membrane plants due to $CaCO_3$ scaling. We focus on two building blocks: Firstly, the improvement of simulation for $CaCO_3$ supersaturation and secondly, a new detection approach with a fibre optic detection system. The latter can be of crucial importance in the validation, calibration and further development of models for the prediction of salt precipitation. The following work gives an overview on the current state of science and technology for the scaling prediction and monitoring. In addition, our new approaches to addressing these challenges are outlined.

In the following publication, Part II, we will then focus on the validation and variation of our prediction model also in the context of scaling data obtained from a full-scale RO plant. In Part III we present results on our optoelectronic fouling sensor with $CaCO_3$ precipitates in a flat membrane cell. In addition, sensor data on other common scales as sulphates will be presented.

2 Prediction of scaling

Scaling describes the precipitation or crystallisation of salt right at the membrane surface during the desalination process. The formation of crystals is only possible if the solution is oversaturated with salts like $CaCO_3$ due to high ion concentrations. When it comes to $CaCO_3$, Ca^{2+} and CO_3^{-2} have to be mentioned, for example. It is common practice in the desalination industry to calculate the salt saturation of concentrated water at the end of the membrane system. Based on this information the process can be designed with respect to feed water recovery. Additionally, the necessary dosage of stabilizing chemicals is connected to the determined saturation. However, a more fundamental prediction of scaling can be found in the thermodynamic principles of nucleation and the growth of crystals. Based on the Gibbs free energy a critical nucleus size has to be overcome for an initialisation of crystallisation and therefore scaling. In this theory, the oversaturation is only one necessary precondition for the formation of a solid crystal. In the following, the current state of science and technology for the description of saturation is presented first. Then we refer to the main aspects of the classical crystallisation theory. This serves as a basis for the goal of predicting $CaCO_3$ scaling in reverse osmosis systems.

2.1 Concept of salt saturation

The precipitation-dissolution behaviour of salt A_mB_n is described in Equation (1). At equilibrium, the law of mass action is applied to derive Equation (2). This describes the equilibrium constant, K, for the ratio between solid and dissolved salt [12, 13].

$$A_mB_{n\,(s)} = m \cdot A^+{}_{(aq)} + n \cdot B^-{}_{(aq)} \qquad \text{(Eq. 1)}$$

$$K = \frac{[A^+]^m \cdot [B^-]^n}{[A_mB_n]} \qquad \text{(Eq. 2)}$$

In order to represent solutions in reality, the thermodynamic term activity α is used instead of concentration (Equation (3)). This term describes an "effective concentration", which considers electrostatic interactions to better reflect non-ideal solutions [2, 14].

$$\alpha = \gamma \cdot c \qquad \text{(Eq. 3)}$$

The activity coefficient γ relates the activity to the concentration c and in water is usually between null and unity [2, 12]. In industrial fresh water treatment processes, generally activity coefficients less than unity can be expected [14]. Therefore, the "effective concentration" involved in the equilibrium relationship usually is less than the actual ion concentration.

The solubility product K of a salt A_mB_n can be expressed via simplification of the equilibrium condition given in Equation (2), whereby the concentration of a pure solid is considered to be constant. This is shown in Equation (4). Additionally, the activity is used rather than concentration, indicated by the use of braces instead of brackets, making it an expression for the thermodynamic solubility product K_S.

$$K_S = \{A^+\}^m \cdot \{B^-\}^n \qquad \text{(Eq. 4)}$$

This expression is valid for both dilute and concentrated solutions due to utilization of activities. Often in literature, the difference between the thermodynamic solubility product K_S and the ideal concentration-based solubility product is not recognized. This leads to errors in the calculation of the saturation state [12, 13, 15].

Up to here, only the description of an equilibrium constant has been addressed. Scaling or crystallisation is generally only possible when real solutions are not in equilibrium. The removal of pure water by reverse osmosis normally leads to salt concentrations that are above equilibrium. The ion activity product (IAP), given by

Equation (5), provides information concerning the current state of a solution not at equilibrium.

$$IAP = \{A^+\}^m \cdot \{B^-\}^n \quad \text{(Eq. 5)}$$

The ratio between the ion activity product and the thermodynamic solubility product describes the saturation of a salt solution. The log_{10} of this ratio, applied to improve the presentation of large number ranges, is the saturation index, as shown in Equation (6) [2].

$$S = \frac{IAP}{K_S} \quad \text{(Eq. 6)}$$

$$SI = log_{10}(S) \quad \text{(Eq. 7)}$$

At SI = 0, the system is in equilibrium. At SI < 0, the solution is unsaturated and solids can be dissolved. At SI > 0, the solution is supersaturated and the precipitation of salt can be expected.

2.2 Polymorphism of $CaCO_3$

Calcium carbonate comes in six different crystal forms. The three anhydrous forms are calcite, aragonite und vaterite [16]. The three hydrated forms are calcium carbonate monohydrate (MCC), amorphous calcium carbonate (ACC) and calcium carbonate hexahydrate (CCH) [17]. It is known that the determination of $CaCO_3$ crystallisation and precipitation all polymorphs are important. Since CCH only occurs rarely, at temperatures near to 0 °C, it is of minor relevance in most cases [18, 19] and is neglected in this work. Calcite shows the lowest solubility, followed by aragonite, vaterite, MCC and lastly ACC. The decisive point in the prediction of precipitation in technical systems is the description of the start of precipitation and its targeted influence. The beginning of the crystallisation is defined by the nucleation, which describes the joining of the smallest molecular units. Nucleation rate is strongly related to surface energy of the nucleus. Since amorphous phases have a relatively low surface energy, nucleation occurs more frequently compared to the crystalline phases. The crystalline phases in turn have a higher stability (lower volume energy), and are therefore increasingly formed in the course of crystal maturation. The transition from amorphous to crystalline structures takes place according to the Ostwald-Lussac rule of stages [20].

2.3 Scaling indices for $CaCO_3$

In order to indicate the saturation of calcite the Langelier Saturation Index (*LSI*) was developed in 1936 and the Stiff & Davis Saturation Index (*S&DSI*) in 1952 [21, 22]. Until today, these indices are widely applied to determine the tendency of solutions to undergo $CaCO_3$ precipitation [23–25]. A great variety to assess the $CaCO_3$ scaling tendency, can be found in literature [23, 25]. A number of these possibilities, along with the much-cited *LSI* and *S&DSI*, are described below.

2.3.1 Langelier Saturation Index: LSI

Based on the work of Tillmans and Heublein (1912) [26], which explored the aggressiveness of carbonic acid, Langelier (1936) [21] developed an index for the determination of the corrosiveness of natural waters. In waters, which are supersaturated with $CaCO_3$, corrosion reactions on surfaces are restricted due to the development of protective scale layers. For waters with a pH between 6.5 and 9.5, Langelier proposed calculating the *LSI* by subtracting a calculated saturation pH value pH_S from the measured pH, as per Equation (8).

$$LSI = pH - pH_{S,calcite} = \Delta pH_{calcite} \quad \text{(Eq. 8)}$$

At *LSI* = 0, the calcium carbonate – carbonic acid system is at equilibrium and no dissolution or precipitation is expected. In waters with a negative *LSI*, calcium carbonate will tend to dissolve, while at positive *LSI*, it will tend to precipitate. The connection between the *LSI* and the more general expression of salt saturation *S* is shown in figure 1.

Langelier proposed a calculation of the *LSI* by using the idealised concentration-based solubility product K_S' which is shown in Equation (9).

$$CaCO_3(s) \Leftrightarrow Ca^{2+} + CO_3^{2-} \qquad K_S' = [Ca^{2+}] \cdot [CO_3^{2-}] \quad \text{(Eq. 9)}$$

As the concentration of CO_3^{2-} is strongly dependent on pH and, in turn, the solubility of $CaCO_3$, it is itself described with an equilibrium as per Equation (10).

$$HCO_3^- \Leftrightarrow H^+ + CO_3^{2-} \qquad K_2' = \frac{[H^+] \cdot [CO_3^{2-}]}{[HCO_3^-]} \quad \text{(Eq. 10)}$$

Equation (9) and (10) both contain the concentration of CO_3^{2-}, thus combination of the equations and resolution according to the H^+ concentration can be made. As pH is defined as $-log_{10}\{H^+\}$, the logarithm of the remaining terms in the combined equation is also

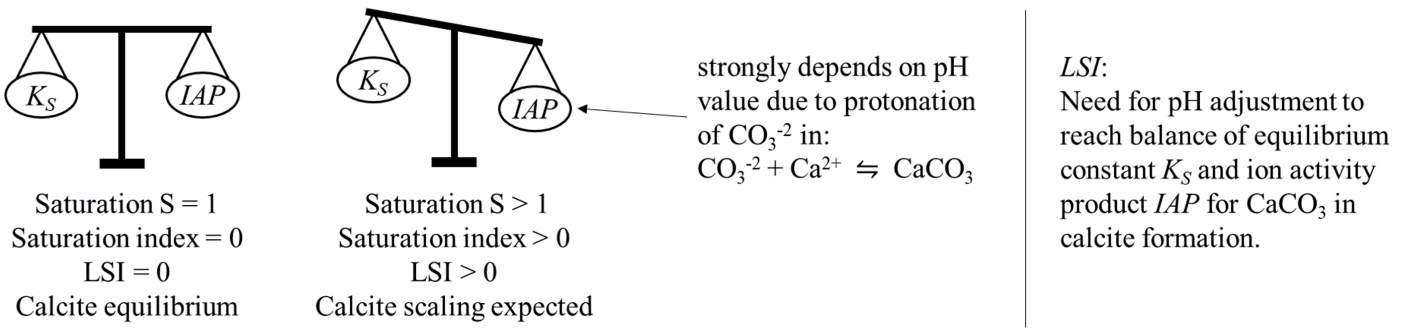

Fig. 1 Connection between the general expression of salt saturation and the Langelier Saturation Index *LSI*

taken, as in pH, designated with the precursor *p*. The resulting equation, shown in Equation (11), allows the calculation of the saturation pH, pH_S.

$$pH_S = (pK_2' - pK_{S,Calcite}') + p\{Ca^{2+}\} + p\{HCO_3^-\} \quad \text{(Eq. 11)}$$

The concentration of HCO_3^- is usually determined through titration for the alkalinity – which is often associated with HCO_3^- concentration. Since alkalinity is known, p{Alk} is used instead of p{HCO_3^-} in Equation (11).

In both reactions, the dissociation of $CaCO_3$ (K_S') is dependent on temperature. To account for this effect, Langelier included an empirical correction of the equilibrium constant. A further correction of the equilibrium constant was undertaken based on activity, which alongside the determination of activity coefficients through the ionic strength, takes the impact of variation in the salt content into account. The calculation of the activity coefficients for the *LSI* is realised with Brönsted-La Mer simplification of the Debye-Hückel-Equation. The validity of this approach is limited to a maximum ionic strength of 20 mmol/L. In comparison, common values for German ground water are 10 and 15 mmol/L [24, 27], whereas sea water can reach 600 mmol/L [28].

2.3.2 LSI as industry standard (ASTM and DIN)

In the literature, the calculation of the *LSI* is mostly done after the current version of the international standard (ASTM) for the Calculation and Adjustment of the Langelier Saturation Index for Reverse Osmosis [11, 23, 29–32]. As in Langelier's original work, the ASTM provides only limited thermodynamic corrections. The effect of temperature and concentration on the equilibrium constant and ion activity is done by graphical approximation. Unfortunately, the ASTM does not provide any physicochemical background information for the proposed corrections.

A more fundamental approach can be found in the most recent standard method applied in the German industry (DIN) for the calculation of calcite saturation [33]. In this work, the pH_S is calculated including a complex chemical background. The impact of temperature is incorporated through the Van't-Hoff-Equation, which is applied to the equilibrium constants. An ion specific calculation of activity is undertaken with the simplified Debye-Hückel-Equation. A further fundamental modification is the inclusion of fourteen complexation reactions and six additional dissociation reactions to Equations (9) and (10) in the calculation of the calcite saturation [33]. This approach, unlike the original *LSI*, cannot be solved algebraically but instead requires an iterative solution. For the verification of an applied calculation routine, the DIN gives a validation data set with 10 different waters.

Despite the possible improvements to the original *LSI*, a very simplified calculation of *LSI* is often applied, albeit with a variation of the temperature and activity corrections. Further reactions, as in the DIN, are often ignored with this approach [23, 30, 34]. The *LSI* is essentially always based on the two chemical equilibriums in Equations (9) and (10), which Langelier previously identified as being relevant in the lime / carbonic acid equilibrium.

2.3.3 S&DSI

As the tendency for $CaCO_3$ precipitation could not be determined in solutions with high ionic strength (high salt content), an extension of the *LSI*, the *S&DSI*, was developed by Stiff and Davis in 1952 [22]. The *S&DSI* is based on the same principles as the *LSI* in Equation (8) and sees application in sea water, process water and oil production, for example. In the calculation of the saturation pH, the term containing the equilibrium constants ($pK_2' - pK_S'$) from Equation (11) is replaced with *K*, resulting in Equation (12).

$$S\&DSI = pH - K - p\{Ca^{2+}\} - p\{Alk\} \quad \text{(Eq. 12)}$$

The empirical constant K has been determined by bringing a number of synthetic waters with varying ionic strength into equilibrium with $CaCO_3$ at temperatures of 0, 30 and 50 °C. As the *S&DSI* is null at equilibrium, Equation (12) was used to solve for K. For the temperatures 10, 20, 25, 40, 60, 70, 80 and 90 °C, the curves were interpolated or extrapolated. The exact derivation process of the original manuscript cannot be reproduced, however. The *S&DSI* generally provides lower values of supersaturation than the *LSI*. The larger the ionic strength, the greater the discrepancy between the two [35]. One obvious explanation for this behaviour could be the limited correction of ion activities with high salt content in the *LSI*.

2.3.4 RSI

In addition to the *LSI* und *S&DSI*, the Ryznar Stability Index (RSI) [36] also gains mention in literature. Equation (13) contains the same terms as the *LSI* or the *S&DSI*, but differs in that the saturation pH is given a larger weighting by a factor of two. The saturation pH is calculated as per the *LSI*.

$$RSI = 2 \cdot pH_{S,Calcite} - pH \quad \text{(Eq. 13)}$$

The basic premise of the *RSI* is the understanding that waters with the same *LSI* can experience different levels of $CaCO_3$ precipitation. Ryznar developed this index following the observation that different waters with the same positive *LSI* showed different corrosiveness. The *LSI* does not determine how much $CaCO_3$ precipitates and thereby did not reflect the resulting variation of the effectiveness of the protective layer which forms [36]. Based on chemical equilibrium the concentration of HCO_3^- und Ca^{2+} must be relatively high if the saturation pH is low and vice versa. Therefore, a different amount of $CaCO_3$-layer forms, which inhibits corrosion of the underlying material more or less. Ryznar included this understanding of the impact of the saturation pH on the expected degree of scaling in the index through the factor two on this term. As defined by Ryznar, precipitation can be expected with an RSI of six or higher. He based this conclusion on empirical data of scaling layer thickness in city pipe systems.

2.3.5 MSLI

The monohydrate *LSI*, or *MSLI*, is a saturation index based on monohydrate calcium carbonate (MCC) [37]. Elfil und Roques (2004) [38] showed that, at different levels of concentration between the solubility equilibrium of MCC and calcite, a metastable zone forms in which crystallisation occurs only when crystallisation seeds are

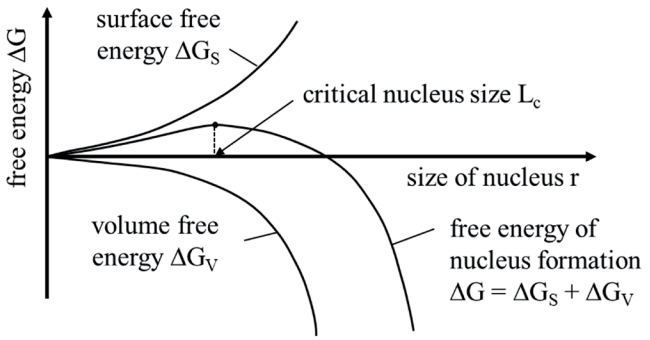

Fig. 2 Free energy of nucleation according to the classical crystallisation theory [39]

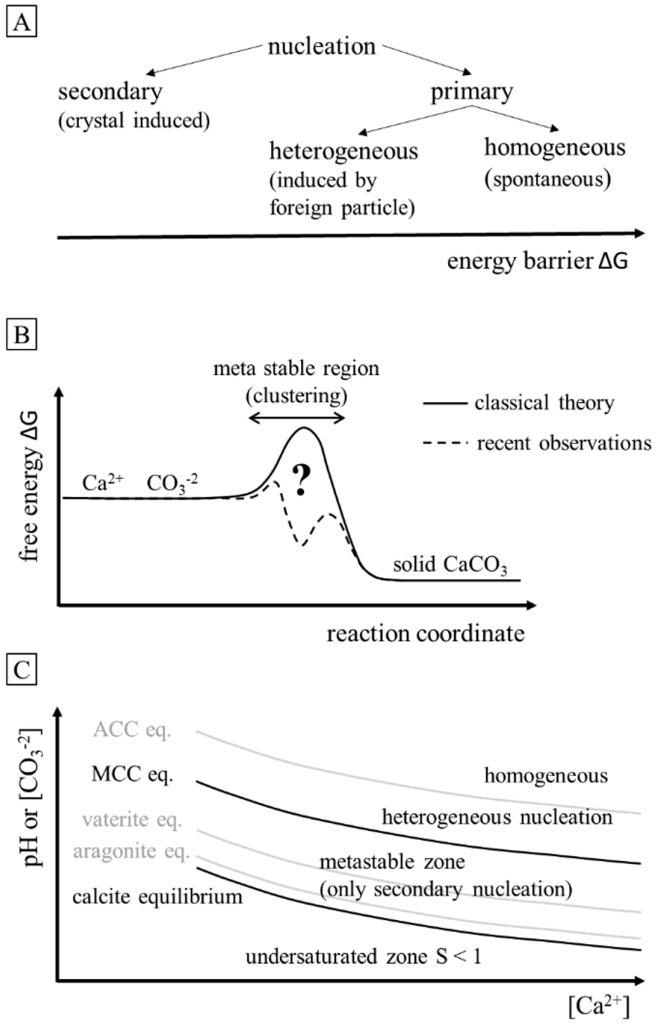

Fig. 3 (A) The role of nucleation pathways [39], (B) free energy [42] and (C) saturation of different polymorphs for the crystallisation of $CaCO_3$ [38]

present. In solutions where the supersaturation is higher than the solubility equilibrium of MCC, spontaneous crystallisation occurs. Accordingly, the *MSLI* describes the thermodynamic equilibrium which, when exceeded, results in spontaneous crystallisation (primary nucleation).

In the *MSLI*, the solubility product of MCC is applied rather than that of calcite, as per Equation (13) and (14).

$$pH_{S,MCC} = pK_2 - pK_{S,MCC} + p\{Ca^{2+}\} + p\{HCO_3^-\} \quad \text{(Eq. 14)}$$

$$MLSI = pH - pH_{S,MCC} = \Delta pH_{MCC} \quad \text{(Eq. 15)}$$

Elfil und Hannachi [37] showed in laboratory environment that water which lies within the metastable zone is not properly described by the *LSI*. The *MSLI*, on the other hand, shows conformity between the index and experimental conclusions at supersaturation with ion activity products less than K_{MCC}. As the solubility product of MCC is larger than that of calcite, the *MSLI* gives smaller values than the *LSI*. Therefore, a smaller scaling potential is predicted.

2.4 Crystallisation theory

As seen from the information above the prediction of scaling is mostly based on more or less simple calculations of chemical equilibria. However, for an accurate description and prediction of crystallisation the oversaturation of a salt can only be a necessary but not a sufficient condition. According to classical crystallisation theory, the relationship between saturation S and free energy ΔG is represented by the basic equations (16)-(18). As depicted in figure 2 the driving force for nucleation is the free energy of the reaction ΔG, which is composed of the surface energy ΔG_S and the volume energy ΔG_V. As shown in equations (16) the surface free energy ΔG_S increases with the interfacial tension γ_n between the crystal surface and the surrounding solution as well as with the surface of the crystal nucleus A_n. It is to be added to the system and is therefore positive. In contrast, the change in the free volume energy ΔG_V is released by solid phase formation and is therefore negative. The change in the free volume energy ΔG_V is proportional to the volume of the nucleus V_n and its concentration c_n and gets greater the greater the energy from temperature *T* and saturation *S* [39, 40].

$$\Delta G_S = A_n \cdot \gamma_n \quad \text{(Eq. 16)}$$

$$\Delta G_V = -V_n \cdot c_n \cdot R \cdot T \cdot \ln S \quad \text{(Eq 17)}$$

$$\Delta G = \Delta G_S + \Delta G_V \quad \text{(Eq. 18)}$$

From a thermodynamic point of view, due to the formation of new surfaces, an energy barrier has to be overcome to start the growing of crystals as shown in figure 3 (A,B). The initial nucleation is the key for an understanding of the existence of oversaturated solutions that do not tend to crystallise. If salt-specific crystals are already present or added to a solution, the so-called secondary nucleation takes place. A primary nucleation requires more energy and therefore higher saturation values. However, more recent observations show a major inadequacy of the classical crystallisation theory for the case of $CaCO_3$. Gebauer et al. showed that the crystallisation of $CaCO_3$ follows a non-classical pathway [41, 42] as illustrated in figure 3 B. Today, new or advanced theories are under discussion for an appropriate description of the nucleation pathway [43, 44]. Despite the missing validation of a consistent theory applicable for the precipitation of $CaCO_3$, Elfil et al. [38, 45] were able to char-

acterise the scaling tendency and metastability based only on the saturation values of the different polymorphs of $CaCO_3$ (Fig. 3 C). They showed that calcite could be highly oversaturated without any precipitation. Only when the monohydrate calcite (MCC) got oversaturated salt precipitations could be detected. Between the calcite and MCC saturation, a metastable region was identified where no precipitation occurred. Between the saturation of MCC and ACC predominately a heterogeneous and wall nature depended precipitation took place. For example, a different precipitation behaviour could be observed on polyamide surfaces compared to steel or glass surfaces. Above the ACC saturation, mainly a strong and spontaneous (homogeneous) nucleation was detected without dependence on the surrounding surfaces. In other words, only when the MCC gets oversaturated a $CaCO_3$ precipitation has to be expected. If the saturation rises even above the ACC saturation it comes to a strong and wall nature independent precipitation. Calcite as the most stable polymorph is often found as the final crystalline structure after the maturation process.

2.5 Hydrochemical simulation software

Hydrochemical simulation software are mostly based on the calculation of chemical equilibria. As described above in connection with the *LSI*, other reactions besides equations (9) and (10) should be considered for the correct description of calcite saturation. In the original paper on the *LSI*, Langelier even addressed this shortcoming due to lack of computing power. One approach overcoming this problem is given in the calculation rule of the German industry (DIN). The broader calculation basis is required to ensure a passably accurate determination of the calcite saturation [33]. Open source simulation software, such as PHREEQC [46], use even more extensive databases and therefore apply additional reactions compared to the DIN. This allows for a comprehensive depiction of water chemistry [2]. A further advantage of such software tools in comparison to pure scaling indices like the *LSI* and *S&DSI*, is the possibility to calculate the quantities of species that must dissolve or precipitate to achieve equilibrium. Therefore, a prediction of a scale mass density is possible. Besides $CaCO_3$ hydrochemical modelling software can determine the saturation state of other minerals frequently associated with scaling issues such as $CaMg(CO_3)_2$, $CaSO_4$, $BaSO_4$, SiO_2 and CaF_2 [47].

2.6 Proposed model for a new $CaCO_3$ scaling index for reverse osmosis systems

Based on the literature on scaling indices and crystallisation theory, we propose a new method for predicting $CaCO_3$ scaling. As shown above, the $CaCO_3$ polymorphism is of decisive importance. In addition to calcite, the MCC and ACC should be considered in particular for a precipitation prognosis in technical systems that are free of seed crystals. The MCC saturation shows the range in which heterogeneous and rather moderate scaling must be expected. Exceeding the ACC saturation marks the beginning of strong precipitation phenomena, which should be largely homogeneous. If seed crystals are present, the calcite equilibrium seems sufficient for predicting $CaCO_3$ precipitation. Preferably, membrane systems should be free of any crystal deposits. The saturation S_{MCC} or its logarithmic scale SI_{MCC} could be of great use to determine the precipitation limit. Since these parameters are not common in industrial environment an expression of the saturation state using *ΔpH* values as with the *LSI* or *MSLI* seems reasonable. There are some shortcomings with the original *LSI* and partly *MSLI* [37] that can be overcome by the application of the hydrochemical software PHREEQC. In particular, calculations for correcting activity and temperature influences reflect the current state of knowledge. Widespread databases are updated by a broad scientific community and allow for the calculation of real waters besides rather simple water matrices. Another major advantage of using the PHREEQC software is the connection of the gas phase with the water chemistry. The different carbon species, from gaseous CO_2 to CO_3^{-2}, and its equilibria play an important role in the formation of $CaCO_3$. Gases such as CO_2 are expected to highly permeate through commonly used polyamide reverse osmosis membranes [48]. Therefore, in addition to pure water, a removal of carbon in the form of CO_2 must also be taken into account in membrane systems. According to the international standard ASTM, a constant CO_2 concentration should be assumed from the feed to the retentate water [32]. In figure 4 we show an example of the structure and programme code of the simulation

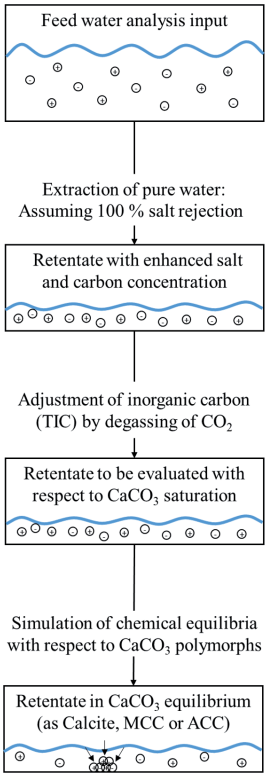


```
SOLUTION 1 feed_water_input
pH 7.31;  temp 12.2;  units mg/L
Ca 120; Mg 19; Na 5.6; K 1.4
Cl 25; N(5) 30 as NO3-; S(6) 27 as SO4-2
alkalinity 372 as HCO3-
END
#Output: CO2 concentration of feed water

USE SOLUTION 1 pure_water_extraction
REACTION; H2O -1.0; 43.298 moles
SAVE solution 11
END
#Phreeq calculates a solution as 1 kg water
containing 55.51 moles pure H20. For example,
a feed water recovery of 78% results in
43.298 moles H20 to be withdrawn.

USE SOLUTION 11 set_CO2_as_in_SOLUTION1
EQUILIBRIUM_PHASES; Fix_CO2 -3.1403
SAVE solution 111
END
#value derived from feed water CO2 SOLUTION 1
log(-CO2[mol/kg]) -> log(-7.239e-04)=-3.1403
#Output: saturation S and SI values
#Output: predicted pH value of the retentate

USE solution 111 set_equilibrium_calcite
EQUILIBRIUM_PHASES; Calcite 0.0  ;END
USE solution 111 set_equilibrium_monohydrate
EQUILIBRIUM_PHASES; MCC 0.0      ;END
USE solution 111 set_equilibrium_amorphous
EQUILIBRIUM_PHASES; ACC 0.0      ;END

#Output: pH values at CaCO3 saturation pHs
```

Fig. 4 Proposed model for the evaluation of $CaCO_3$ scaling indices for reverse osmosis retentates applying PHREEQC software. The left side shows an example including major elements of a script for the calculation of saturation values and *ΔpH* values like the *LSI* or *MSLI*

Table 1 Comparative overview of approaches for the prediction of CaCO3 scaling in reverse osmosis systems:

	LSI original	LSI ASTM	LSI based on DIN	S&DSI original	RSI	MSLI	Classical crystallisation theory	Our proposed simulation model (PHREEQC)
Salinity: Intended use for high or low salinity (calculation methods and chemistry database)	low	low	low	high	low	low	both possible*	both (database dependent)
Based on surface and volume free energy: Fundamental energy considerations	–	–	–	–	–	–	✓	–
Validation: Currently recognised as valid/sufficient in the respective field of application	✓	✓	✓	✓	✓	✓	–	to be proven
Chrystal growth: Description of crystal growth besides principal crystallisation indication	–	–	–	–	–	–	✓	–
Database maintenance: Further development of data basis by the scientific community	–	–	–	–	–	–	–	✓
Comprehensive water chemistry: Beside carbonate chemistry e.g. sulphate and phosphate as well as complexation reactions are considered	–	–		–	–	–	–	✓
No restriction on $CaCO_3$: Applicable to other salts as $BaSO_4$, $SrSO_4$, $CaMg(CO_3)_2$ etc.	–	–	–	–	–	–	possible*	✓
High quality correction of the standard conditions: Correction of temperature and ion activity according to the state of science	–	–	✓ limited	–	–	–	possible*	✓
Metastability considered: Application in seed crystal-free environments reasonable	–	–	–	–	–	✓	✓	✓
Polymorphism (especially calcite, MCC and ACC equilibria): Consideration of the polymorphism of $CaCO_3$	–	–	–	–	–	✓	possible*	✓
CO_2 degassing: Applicability in membrane technology by describing carbonate chemistry in terms of CO_2 permeation through the membrane	–	✓	–	–	–	–	possible*	✓

*possible with a combination of calculations based on the description of chemical equilibria – e.g. our proposed simulation model

model for the evaluation of $CaCO_3$ scaling indices for reverse osmosis with the PHREEQC software.

The exemplary code modules shows a simplification of the membrane system by assuming 100 % salt rejection and constant CO_2 concentration in the retentate water. Both assumptions are commonly applied for the design of membrane systems. Design software provided by membrane suppliers usually calculates ion specific salt rejection of different membranes. For the calculation of the *LSI* or the scaling tendency, this error is usually negligible [32] and plays a more important role for the prediction of the permeate chemistry. However, for a more accurate calculation the model depicted in figure 4 allows for an adjustments of ion specific rejection rates. Instead of the extraction of pure water, element specific removal rates would have to be implemented following the key word REACTION. An essential part of the model is the calculation of CO_2 gas exchange through the membrane. A reasonable customization could be an extraction of CO_2 content present in the feed water instead of applying a constant CO_2 concentration as show with the example in figure 4. Due to carbonic equilibria, the pH value of a solution is highly dependent on the CO_2 concentration and allows for a validation of the assumption made for CO_2. If the measured and simulated pH value are not in accordance, a reverse modelling for the adaption of real CO_2 extraction can be applied. Besides the saturation state of $CaCO_3$ other relevant salts can be found in the PHREEQC output files. Depending on the applied database the saturation of calcium sulphate ($CaSO_4$), barium sulphate ($BaSO_4$), strontium sulphate ($SrSO_4$), dolomite ($CaMg(CO_3)_2$), or calcium fluoride (CaF_2) can be analysed for example.

2.7 Comparison of the different approaches to predicting $CaCO_3$ precipitation

Only when $CaCO_3$ seed crystals are present, the calcite equilibrium appears to be sufficient for predicting $CaCO_3$ precipitation. In this case, no metastable zone is formed and the secondary crystallisation process will reduce the supersaturation of the solution until the calcite supersaturation is eliminated (Fig. 3 C). At least when new, membrane systems should be clean and free of seed crystals. If, in addition, the ACC solubility is not exceeded, it can be assumed that the metastable zone also serves as protection against $CaCO_3$ precipitation. Calcite saturation can be greatly exceeded in this case. The MCC saturation can then provide an important orientation for the design of the maximum targeted concentration in RO plants. If the ACC equilibrium is exceeded, violent and spontaneous precipitation is to be expected and thus forms another important orientation for process design. A comparative overview of all presented approaches for predicting $CaCO_3$ scaling in RO systems is shown in table 1.

3 Detection of Scaling

The foregoing has shown how to theoretically approach the prediction of $CaCO_3$ scaling and that there are significant gaps in a comprehensive description. For further development and verification of accurate prediction in RO systems and subsequent progress, an efficient monitoring system is crucial. In the following, we briefly show the state of the art in science and technology for the technical monitoring of scaling in membrane systems. In addition, we present our new approach for monitoring membrane systems using optoelectronic measurement technology.

3.1 Technical devices for fouling detection in reverse osmosis systems

For industrial use, RO membranes are generally provided in compactly assembled membrane modules, mostly as spiral wound modules. To hold the membranes at a distance and allow for evenly distributed flow through the module, net-type spacers are placed between the membrane sheets. At the feed water side of the membrane, spacers at a height of 600 – 900 µm are generally used, forming feed channels that are prone to the accumulation of deposits as salt precipitations [49]. Each feed medium contains different substances that can cause fouling within the feed channel and directly on the membrane. As illustrated in table 2, fouling phenomena or membrane failure can generally be distinguished along with their prevalence in different membrane applications.

Determining the prevalent type of fouling is essential for its prevention and therefore process stability. However, in many cases, identification of the type of fouling is a complex interplay of different information. For instance, normalised membrane plant performance data and the visual inspection of susceptible elements may be necessary, as well as an element autopsy for the exact determination of the type of fouling [10]. Often a understanding of fouling and its effects on plant performance data is hardly given [50]. Table 3 provides an overview of methods that can be used for in situ fouling detection.

Table 2: Ranking of three most frequent types of fouling or membrane failure depending on the type of membrane application [10]

Incidence	Low Pressure RO (brackish and fresh water)	High Pressure RO (seawater)
+++	Scaling	Biofouling
++	Organic and colloidal fouling	Organic and colloidal fouling
+	Biofouling	Oxidation

A comparable overview to table 3 was produced by Chen et al. in 2004 [83] and Sim et al. in 2013 [84]. In comparison, we included in table 3 techniques applied at a later stage, as Raman spectroscopy and optical coherence tomography. Our overview demonstrates that some of these methods have not been applied with spiral wound modules. Ultrasonic time domain reflectometry has only been successfully used in the presence of inorganic foulants and magnetic resonance for the detection of biofouling. Recently, Karabelas et al. [11] highlighted the need for a "sensitive and reliable scale detection and monitoring method" for reverse osmosis systems.

3.2 Proposed optical measuring technique for scaling detection

In table 3, we distinguish between flat membrane and spiral wound membrane applications. As indicated in table 3, there is no comprehensive fouling detection applicable to main foulants and membrane modules. Therefore, we developed a new technology that is based on the integration of a minimally invasive polymer optical fibre (POF) into the feed spacer. POFs and glass fibres have already been successfully tested for the detection of different precipitates, such as scales and biofouling [85–89]. Our approach has the potential to meet all of the requirements of membrane applications defined in table 3.

POFs are normally used in optical data links. Figure 5, see page 130, illustrates the detection principles for salt precipitation and biofouling. We propose the use of standard polymethylmethacrylate (PMMA) step-index POF with common diameters of 250, 500 or

Table 3 Overview of methods for an in situ membrane fouling detection

Method	Examples and technical features	Biofouling	Scaling	Flat membrane cell	Spiral wound module	Source
Optical	High-resolution imaging with a camera through a transparent flat membrane cell, applications using colour tracers, oxygen optodes, optical coherence tomography and laser-based technologies.	✓	✓	✓	–	[51–60]
Electrical impedance	Electrodes placed at a special flat membrane cell used for the detection of changes in electrical impedance and thus the fouling state.	✓	✓	✓	–	[61–70]
Ultrasonic	Shifts in ultrasonic reflections can be used to detect inorganic precipitates.	–*	✓	✓	✓	[71–80]
Magnetic resonance	Tracking of hydrogen atoms and thus the estimation of stagnant zones in water flow, which leads to local fouling determination.	✓	–	✓	✓	[81, 82]

* Except for biofouling spiked with inorganics

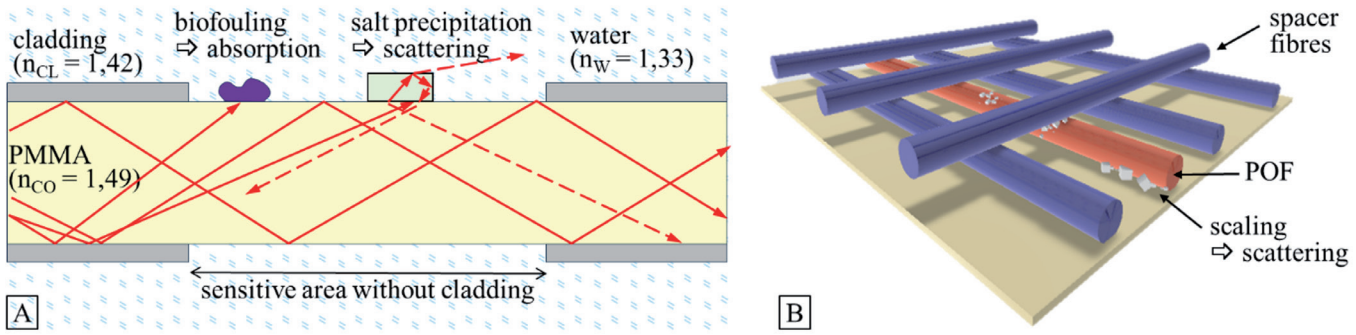

Fig. 5: Polymer optical fibre with partially removed cladding for fouling detection (A). Example for the integration of a POF with sensitive surface into a feed spacer and illustration of salt deposits at relevant locations for an interaction with guided light (B)

1000 µm. To produce a sensitive section, the 10 µm thick fluoropolymer cladding must be removed. This allows for an interaction of guided light inside the core and foulants on the core surface. As water and the cladding have refractive indices n lower than that of the PMMA core, both can maintain total reflection of light. Interaction between light and the precipitate occurs as foulants come into contact with the exposed fibre core. This process usually results in the loss of guided light by absorption, scattering or frustration of the total internal reflection [85–89].

The required optoelectric setup is shown in figure 6. Basically, the measurement requires a light-emitting diode (LED) as light source, a polymer optical fibre (POF) as sensor and a photodiode as detector. Red LEDs are commonly used for data communication with POFs due to the low attenuation and a widespread availability of suitable LEDs [90]. If a wavelength-dependent interaction of fouling and guided light has to be expected the complete visual spectrum can be evaluated white light source and a spectrometer. Calcite as example has a white appearance which is caused by a homogeneously scattered light of all visible light wavelength [91]. Therefore, the utilisation of a red-light LED and an optometer can be a cost-effective choice.

4 Conclusion

With this study, we have shown that the prediction of $CaCO_3$ scaling for reverse osmosis systems is widely based on indices as the *LSI*. This index describes the chemical equilibrium of calcite by indicating the pH value difference between equilibrium and the actual solution state. This approach is based on simplifications of the water chemistry and does not reflect the current state of knowledge and the relevance of the $CaCO_3$ polymorphism. Alternative scaling indices as the *S&DSI* and the RSI are solely derivations with defined deviations from the *LSI* and therefore do not offer any basic improvements. In recent years, the classical crystallisation theory was identified as not applicable to the crystallisation of $CaCO_3$. Other theories are not validated to date and currently under discussion. The major challenge lies in the description of the metastable zone of a $CaCO_3$ supersaturated solutions. This means that $CaCO_3$ can be widely supersaturated without precipitation occurring. However, the chemical equilibrium of a hydrated form of $CaCO_3$ seem to aptly describe the upper limit of the metastable zone. It was found that the supersaturation of the monohydrate calcite (MCC) limits the metastable range. Applying the MCC equilibrium with a combination of our developed hydrochemical simulation model for a reverse osmosis (RO) process gives a promising tool for an improved prediction of $CaCO_3$ precipitation. The depicted influence of CO_2 permeation through the membrane must be emphasised here, since the solubility of $CaCO_3$ is strongly related to it through a shift in the pH value and therefore concentration of CO_3^{-2}. In addition, a comprehensive calculation of water chemistry with the software PHREEQC, which is maintained by the scientific community, enables reliable simulations. Our simulation model is intended for the prognosis of salt precipitation on the basis of the saturation state of salts such as $CaCO_3$ in a reverse osmosis concentrate. The saturation is an important but not sufficient information for a comprehensive energetic but today still uncertain description of $CaCO_3$ crystallisation. Furthermore, the literature shows that reliable monitoring of scaling is required. The optoelectronic monitoring of salt precipitation in RO systems can finally serve to verify and further develop prediction models. Both, our simulative and measuring approach have the potential to enable demand-oriented control and design of reverse osmosis processes. Techno-economic and ecological progress in water treatment using RO could be made possible by applying our suggestions. The following parts II and III deal with model variation and validation as well as with results on scaling detection using the fibre optic sensor.

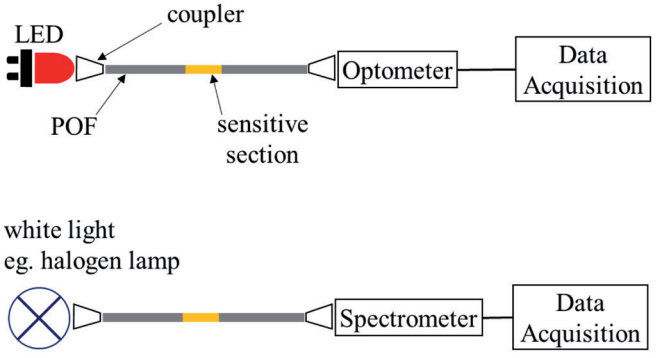

Fig. 6 Optoelectronic measurement for scaling detection with polymer optical fibres (POF)

5 References

1. Greenlee, L. F.; Lawler, D. F.; Freeman, B. D.; Marrot, B. and Moulin, P.: Reverse osmosis desalination: water sources, technology, and

today's challenges, Water research, **43** (2009), no. 9, pp. 2317-2348.
2. Appelo, C. A. J. and Postma, D.: Geochemistry, groundwater and pollution, 2nd ed., CRC Press, Boca Raton, 2013.
3. MacAdam, I. and Iarvis, P.: Water-Formed Scales and Deposits: Types, Characteristics, and Relevant Industries, in Amjad, Z. and Demadis, K. D. (Eds.): Mineral scales and deposits: Scientific and technological approaches, Elsevier, Amsterdam, 2015, pp. 3-23.
4. Gilron, J.: Brine Treatment and High Recovery Desalination, Emerging Membrane Technology for Sustainable Water Treatment, Elsevier, 2016, pp. 297-324.
5. Feiner, M.; Beggel, S.; Jaeger, N. and Geist, J.: Increased RO concentrate toxicity following application of antiscalants – acute toxicity tests with the amphipods Gammarus pulex and Gammarus roeseli, Environmental pollution, **197** (2015), pp. 309-312.
6. Stetter, D.; Panglisch, S. and Dördelmann, O.: Abschlussbericht W 201502: Entwicklung eines erweiterten Monitoringkonzepts zur Überwachung der Wasserqualität von RO/NF-Anlagen, 2015.
7. Panglisch, S.: Geschäftsführung der Deutschen Gesellschaft für Membrantechnik: Schadstoff aus Antiscalants in Umkehrosmose Permeaten, mündlich, April 15th 2021.
8. van de Lisdonk, C.A.C.; Rietman, B. M.; Heijman, S.; Sterk, G. R. and Schippers, J. C.: Prediction of supersaturation and monitoring of scaling in reverse osmosis and nanofiltration membrane systems, Desalination, **138** (2001), no. 1-3, pp. 259-270.
9. Oh, H.-J.; Choung, Y.-K.; Lee, S.; Choi, J.-S.; Hwang, T.-M. and Kim, J. H.: Scale formation in reverse osmosis desalination: Model development, Desalination, **238** (2009), no. 1-3, pp. 333-346.
10. Wilf, M.: Membrane-Based Desalination Processes: Challenges and Solutions, in Amjad, Z. and Demadis, K. D. (Eds.): Mineral scales and deposits: Scientific and technological approaches, Elsevier, Amsterdam, 2015, pp. 477-497.
11. Karabelas, A. J.; Mitrouli, S. T. and Kostoglou, M.: Scaling in reverse osmosis desalination plants: A perspective focusing on development of comprehensive simulation tools, Desalination, **474** (2020), p. 114193.
12. Mortimer, C. E.; Müller, U. and Beck, J.: Chemie: Das Basiswissen der Chemie, 11th ed., Thieme, Stuttgart, 2014.
13. Atkins, P. W.; Paula, J. de and Ludwig, R.: Kurzlehrbuch physikalische Chemie, 4th ed., Wiley-VCH, Weinheim, 2008.
14. Wilhelm, S.: Wasseraufbereitung: Chemie und chemische Verfahrenstechnik, 7th ed., Springer-Verlag, Berlin, Heidelberg, 2008.
15. Holleman, A. F.; Wiberg, E. and Wiberg, N.: Lehrbuch der anorganischen Chemie, 102nd ed., De Gruyter, Berlin, 2007.
16. Plummer, L. and Busenberg, E.: The solubilities of calcite, aragonite and vaterite in CO_2-H_2O solutions between 0 and 90°C, and an evaluation of the aqueous model for the system $CaCO_3$-CO_2-H_2O, Geochimica et Cosmochimica Acta, **46** (1982), no. 6, pp. 1011-1040.
17. Tlili, M. M.; Amor, M. B.; Gabrielli, C.; Joiret, S.; Maurin, G. and Rousseau, P.: Characterization of $CaCO_3$ hydrates by micro-Raman spectroscopy, Journal of Raman Spectroscopy, **33** (2002), no. 1, pp. 10-16.
18. Bischoff, J. L.; Fitzpatrick, J. A. and Rosenbauer, R. J.: The solubility and stabilization of ikaite ($CaCO_3$·$6H_2O$) from 0 to 25 °C: Environmental and paleoclimatic implications for thinolite tufa, Journal of Geology, **101** (1993), no. 1, pp. 21-33.
19. Brečević, L.; Nielsen, A. E.; Oskarsson, Å.; Hewitt, G. M.; Kutney, J. P.; Li, K. et al.: Solubility of Calcium Carbonate Hexahydrate, Acta Chemica Scandinavica, 47 (1993), pp. 668-673.
20. Wolf, S. E. and Gower, L. B.: Challenges and Perspectives of the Polymer-Induced Liquid-Precursor Process: The Pathway from Liquid-Condensed Mineral Precursors to Mesocrystalline Products, in van Driessche, A. E.; Kellermeier, M.; Benning, L. G. and Gebauer, D. (Eds.): New Perspectives on Mineral Nucleation and Growth, Springer International Publishing, Cham, 2017, pp. 43-75.
21. Langelier, W. F.: The analytical control of anti-corrosion water treatment, Journal - American Water Works Association, **28** (1936), no. 10, pp. 1500-1521.
22. Stiff, H. A. and Davis, L. E.: A Method for Predicting the Tendency of Oil Field Waters To Deposit Calcium Carbonate, Journal of Petroleum Technology, **4** (1952), no. 09, pp. 213-216.
23. Antony, A.; Low, J. H.; Gray, S.; Childress, A. E.; Le-Clech, P. and Leslie, G.: Scale formation and control in high pressure membrane water treatment systems: A review, Journal of Membrane Science, **383** (2011), 1-2, pp. 1-16.
24. Gimbel, R.; Jekel, M. and Ließfeld, R. (Eds.): Wasseraufbereitung – Grundlagen und Verfahren, 1st ed., Oldenbourg Industrieverlag, München, 2004.
25. Huang, Q. and Ma, W.: A model of estimating scaling potential in reverse osmosis and nanofiltration systems, Desalination, **288** (2012), pp. 40-46.
26. Tillmans, J. and Heublein, O.: Investigation of the Carbon Dioxide which Attacks Calcium Carbonate in Natural Waters, Gesundheits-Ingenieur, **35** (1912), pp. 669-677.
27. Schöpke, R.: Hydrochemie der Wasseraufbereitung: Begleitmaterial zur Lehrveranstaltung des LS Wassertechnik & Siedlungswasserbau der BTU-Cottbus, lecture notes, 2012, http://www-docs.tu-cottbus.de/wassertechnik/public/Skripte/Vorlesung/WT2005.pdf, accessed July 2, 2015.
28. Yang, J.; Lee, S.; Lee, E.; Lee, J. and Hong, S.: Effect of solution chemistry on the surface property of reverse osmosis membranes under seawater conditions, Desalination, **247** (2009), no. 1-3, pp. 148-161.
29. Crittenden, J. C.; Trussell, R. R.; Hand, D. W.; Howe, K. J. and Tchobanoglous, G.: MWH's Water Treatment: Principles and Design, 3rd ed., John Wiley and Sons, Hoboken, N.J, 2012.
30. Dow Chemical Company: FILMTEC™ Reverse Osmosis Membranes: Technical Manual, http://msdssearch.dow.com/PublishedLiteratureDOWCOM/dh_08db/0901b803808db77d.pdf?filepath=liquidseps/pdfs/noreg/609-00071.pdf&fromPage=GetDoc, accessed April 9, 2015.
31. Dupont: FilmTec™ Reverse Osmosis Membranes Technical Manual, 2020, https://www.dupont.com/content/dam/dupont/amer/us/en/water-solutions/public/documents/en/45-D01504-en.pdf.
32. ASTM International: Standard Practice for Calculation and Adjustment of the Langelier Saturation Index for Reverse Osmosis D3739 – 19.
33. Deutsches Institut für Normung e. V.: German standard methods for the examination of water, waste water and sludge - Physical and physico-chemical parameters (group C) – Part 10: Calculation of the calcit saturation of water (C 10), 13.060.60, 38404-10:2012-12, Beuth Verlag, Berlin, 2012.
34. Tchobanoglous, G.: Wastewater engineering: Treatment and reuse, 4th ed., McGraw-Hill, Boston, 2003.
35. Sheikholeslami, R.: Scaling potential index (SPI) for CaCO3 based on Gibbs free energies, AIChE Journal, **51** (2005), no. 6, pp. 1782-1789.
36. Ryznar, J. W.: A New Index for Determining Amount of Calcium Carbonate Scale Formed by a Water, Journal - American Water Works Association, **36** (1944), no. 4, pp. 472-486.
37. Elfil, H. and Hannachi, A.: Reconsidering water scaling tendency assessment, AIChE Journal, 52 (2006), no. 10, pp. 3583-3591.
38. Elfil, H. and Roques, H.: Prediction of the limit of the metastable zone in the "$CaCO_3$-CO_2-H_2O" system, AIChE Journal, **50** (2004), no. 8, pp. 1908-1916.

39. Mullin, J. W.: Crystallization, 4th ed., Elsevier professional, s.l., 2001.
40. Gnielinski, V.; Mersmann, A. and Thurner, F.: Verdampfung, Kristallisation, Trocknung, Springer, Berlin, Heidelberg, 1993.
41. van Driessche, A. E.; Kellermeier, M.; Benning, L. G. and Gebauer, D. (Eds.): New Perspectives on Mineral Nucleation and Growth, Springer International Publishing, Cham, 2017.
42. Gebauer, D.; Völkel, A. and Cölfen, H.: Stable prenucleation calcium carbonate clusters, Science (New York, N.Y.), **322** (2008), no. 5909, pp. 1819-1822.
43. Lutsko, J. F.: How crystals form: A theory of nucleation pathways, Science advances, **5** (2019), no. 4, eaav7399.
44. Grosfils, P. and Lutsko, J. F.: Impact of Surface Roughness on Crystal Nucleation, Crystals, **11** (2021), no. 1, p. 4.
45. Elfil, H. and Roques, H.: Role of hydrate phases of calcium carbonate on the scaling phenomenon, Desalination, **137** (2001), 1-3, pp. 177-186.
46. Parkhurst, D. L. and Appelo, C. A. J.: Description of Input and Examples for PHREEQC Version 3: A Computer Program for Speciation, Batch-Reaction, One-Dimensional Transport, and Inverse Geochemical Calculations, book 6, chapter A43, 2013, https://pubs.usgs.gov/tm/06/a43/, accessed March 6, 2017.
47. Melin, T. and Rautenbach, R.: Membranverfahren: Grundlagen der Modul- und Anlagenauslegung, 3rd ed., Springer-Verlag, Berlin, Heidelberg, 2007.
48. Hoek, E. M. V. and Tarabara, V. (Eds.): Encyclopedia of membrane science and technology: Volume 2, Wiley, Hoboken, NJ, 2013.
49. Johnson, J. E.: Design and Construction of Commercial Spiral Wound Modules, in Hoek, E. M. V. and Tarabara, V. (Eds.): Encyclopedia of membrane science and technology: Volume 2, Wiley, Hoboken, NJ, 2013, pp. 1170-1190.
50. Park, S.-M.; Han, J.; Lee, S.; Sohn, J.; Kim, Y.-M.; Choi, J.-S. et al.: Analysis of reverse osmosis system performance using a genetic programming technique, Desalination and Water Treatment, **43** (2012), no. 1-3, pp. 281-290.
51. Vrouwenvelder, J. S.; van Paassen, J. A. M.; Wessels, L.; van Dam, A. F. and Bakker, S.: The Membrane Fouling Simulator: A practical tool for fouling prediction and control, Journal of Membrane Science, **281** (2006), no. 1-2, pp. 316-324.
52. Vrouwenvelder, J. S.; Bakker, S. M.; Cauchard, M.; Le Grand, R.; Apacandié, M.; Idrissi, M. et al.: The membrane fouling simulator: A suitable tool for prediction and characterisation of membrane fouling, Water Science & Technology, **55** (2007), no. 8-9, p. 197.
53. Cohen, Y. and Uchymiak, M.: Method and system for monitoring reverse osmosis membranes, US007910004B2, 2007.
54. Uchymiak, M.; Bartman, A. R.; Daltrophe, N.; Weissman, M.; Gilron, J.; Christofides, P. D. et al.: Brackish water reverse osmosis (BWRO) operation in feed flow reversal mode using an ex situ scale observation detector (EXSOD), Journal of Membrane Science, **341** (2009), no. 1-2, pp. 60-66.
55. Farhat, N. M.; Staal, M.; Siddiqui, A.; Borisov, S. M.; Bucs, S. S. and Vrouwenvelder, J. S.: Early non-destructive biofouling detection and spatial distribution: Application of oxygen sensing optodes, Water research, **83** (2015), pp. 10-20.
56. Farhat, N. M.; Vrouwenvelder, J. S.; van Loosdrecht, M. C. M.; Bucs, S. S. and Staal, M.: Effect of water temperature on biofouling development in reverse osmosis membrane systems, Water research, **103** (2016), pp. 149-159.
57. West, S.; Wagner, M.; Engelke, C. and Horn, H.: Optical coherence tomography for the in situ three-dimensional visualization and quantification of feed spacer channel fouling in reverse osmosis membrane modules, Journal of Membrane Science, **498** (2016), pp. 345-352.
58. Dreszer, C.; Wexler, A. D.; Drusova, S.; Overdijk, T.; Zwijnenburg, A.; Flemming, H.-C. et al.: In-situ biofilm characterization in membrane systems using Optical Coherence Tomography: formation, structure, detachment and impact of flux change, Water research, **67** (2014), pp. 243-254.
59. Wagner, M.; Taherzadeh, D.; Haisch, C. and Horn, H.: Investigation of the mesoscale structure and volumetric features of biofilms using optical coherence tomography, Biotechnology and bioengineering, **107** (2010), no. 5, pp. 844-853.
60. Virtanen, T.; Reinikainen, S.-P.; Kögler, M.; Mänttäri, M.; Viitala, T. and Kallioinen, M.: Real-time fouling monitoring with Raman spectroscopy, Journal of Membrane Science, **525** (2017), pp. 312-319.
61. Antony, A.; Chilcott, T.; Coster, H. and Leslie, G.: In situ structural and functional characterization of reverse osmosis membranes using electrical impedance spectroscopy, Journal of Membrane Science, **425-426** (2013), pp. 89-97.
62. Hu, Z.; Antony, A.; Leslie, G. and Le-Clech, P.: Real-time monitoring of scale formation in reverse osmosis using electrical impedance spectroscopy, Journal of Membrane Science, **453** (2014), pp. 320-327.
63. Bannwarth, S.; Darestani, M.; Coster, H. and Wessling, M.: Characterization of hollow fiber membranes by impedance spectroscopy, Journal of Membrane Science, **473** (2015), pp. 318-326.
64. Bannwarth, S.; Trieu, T.; Oberschelp, C. and Wessling, M.: On-line monitoring of cake layer structure during fouling on porous membranes by in situ electrical impedance analysis, Journal of Membrane Science, **503** (2016), pp. 188-198.
65. Sim, L. N.; Wang, Z. J.; Gu, J.; Coster, H. and Fane, A. G.: Detection of reverse osmosis membrane fouling with silica, bovine serum albumin and their mixture using in-situ electrical impedance spectroscopy, Journal of Membrane Science, **443** (2013), pp. 45-53.
66. Cen, J.; Kavanagh, J.; Coster, H. and Barton, G.: Fouling of reverse osmosis membranes by cane molasses fermentation wastewater: Detection by electrical impedance spectroscopy techniques, Desalination and Water Treatment, **51** (2013), no. 4-6, pp. 969-975.
67. Cen, J.; Vukas, M.; Barton, G.; Kavanagh, J. and Coster, H.: Real time fouling monitoring with Electrical Impedance Spectroscopy, Journal of Membrane Science, **484** (2015), pp. 133-139.
68. Sim, L. N.; Gu, J.; Coster, H. G. and Fane, A. G.: Quantitative determination of the electrical properties of RO membranes during fouling and cleaning processes using electrical impedance spectroscopy, Desalination, **379** (2016), pp. 126-136.
69. Ho, J. S.; Sim, L. N.; Gu, J.; Webster, R. D.; Fane, A. G. and Coster, H. G.: A threshold flux phenomenon for colloidal fouling in reverse osmosis characterized by transmembrane pressure and electrical impedance spectroscopy, Journal of Membrane Science, **500** (2016), pp. 55-65.
70. Ho, J. S.; Low, J. H.; Sim, L. N.; Webster, R. D.; Rice, S. A.; Fane, A. G. et al.: In-situ monitoring of biofouling on reverse osmosis membranes: Detection and mechanistic study using electrical impedance spectroscopy, Journal of Membrane Science, **518** (2016), pp. 229-242.
71. Mairal, A. P.; Greenberg, A. R.; Krantz, W. B. and Bond, L. J.: Real-time measurement of inorganic fouling of RO desalination membranes using ultrasonic time-domain reflectometry, Journal of Membrane Science, **159** (1999), 1-2, pp. 185-196.
72. Bond, L. J.; Chai, G. Y.; Greenberg, A. R. and Krantz, W. B.: Method and Apparatus für Determining the State of Fouling/Cleaning of Membrane Modules, US006161435A, 1999.
73. Mairal, A. P.; Greenberg, A. R. and Krantz, W. B.: Investigation of mem-

brane fouling and cleaning using ultrasonic time-domain reflectometry, Desalination, **130** (2000), no. 1, pp. 45-60.

74. Taheri, A. H.; Sim, S.; Sim, L. N.; Chong, T. H.; Krantz, W. B. and Fane, A. G.: Development of a new technique to predict reverse osmosis fouling, Journal of Membrane Science, **448** (2013), pp. 12-22.
75. Sanderson, R.; Li, J.; Koen, L. J. and Lorenzen, L.: Ultrasonic time-domain reflectometry as a non-destructive instrumental visualization technique to monitor inorganic fouling and cleaning on reverse osmosis membranes, Journal of Membrane Science, **207** (2002), no. 1, pp. 105-117.
76. Zhang, Z.-X.; Greenberg, A. R.; Krantz, W. B. and Chai, G.-Y.: Study of membrane fouling and cleaning in spiral wound modules using ultrasonic time-domain reflectometry, New Insights into Membrane Science and Technology: Polymeric and Biofunctional Membranes, Elsevier, 2003, pp. 65-88.
77. Chai, G.-Y.; Greenberg, A. R. and Krantz, W. B.: Ultrasound, gravimetric, and SEM studies of inorganic fouling in spiral-wound membrane modules, Desalination, **208** (2007), 1-3, pp. 277-293.
78. Chong, T. H.; Wong, F. S. and Fane, A. G.: Fouling in reverse osmosis: Detection by non-invasive techniques, Desalination, **204** (2007), no. 1-3, pp. 148-154.
79. An, G.; Lin, J.; Li, J.; Li, X. and Jian, X.: Non-invasive measurement of membrane scaling and cleaning in spiral-wound reverse osmosis modules by ultrasonic time-domain reflectometry with sound intensity calculation, Desalination, **283** (2011), pp. 3-9.
80. Chai, G. Y.; Cao, B.; Zhao, G. Y.; Greenberg, A. R. and Krantz, W. B.: Effects of concentration polarization, temperature and pressure on ultrasound detection of inorganic fouling and cleaning in a spiral-wound membrane module, Desalination and Water Treatment, **50** (2012), no. 1-3, pp. 411-422.
81. Creber, S. A.; Vrouwenvelder, J. S.; van Loosdrecht, M. and Johns, M. L.: Chemical cleaning of biofouling in reverse osmosis membranes evaluated using magnetic resonance imaging, Journal of Membrane Science, **362** (2010), no. 1-2, pp. 202-210.
82. Fridjonsson, E. O.; Vogt, S. J.; Vrouwenvelder, J. S. and Johns, M. L.: Early non-destructive biofouling detection in spiral wound RO membranes using a mobile earth's field NMR, Journal of Membrane Science, **489** (2015), pp. 227-236.
83. Chen, V.; Li, H. and Fane, A. G.: Non-invasive observation of synthetic membrane processes – a review of methods, Journal of Membrane Science, **241** (2004), no. 1, pp. 23-44.
84. Sim, S.; Suwarno, S. R.; Chong, T. H.; Krantz, W. B. and Fane, A. G.: Monitoring membrane biofouling via ultrasonic time-domain reflectometry enhanced by silica dosing, Journal of Membrane Science, **428** (2013), pp. 24-37.
85. Philip-Chandy, R.; Scully, P. J.; Eldridge, P.; Kadim, H. J.; Grapin, M. G.; Jonca, M. G. et al.: An optical fiber sensor for biofilm measurement using intensity modulation and image analysis, IEEE Journal of Selected Topics in Quantum Electronics, **6** (2000), no. 5, pp. 764-772.
86. Philip-Chandy, R.; Scully, P. and Thomas, D.: A novel technique for on-line measurement of scaling using a multimode optical fibre sensor for industrial applications, Sensors and Actuators B: Chemical, **71** (2000), 1-2, pp. 19-23.
87. Wong, Y. M.; Scully, P. J.; Bartlett, R. J.; Kuang, K. S. C. and Cantwell, W. J.: Plastic Optical Fibre Sensors for Environmental Monitoring: Biofouling and Strain Applications, Strain, **39** (2003), no. 3, pp. 115-119.
88. Wallace, A. D.; Boerkamp, M.; Lye, P. G.; Lamb, D. W.; Doherty, W. O. S. and Fellows, C. M.: Assessment of an Intrinsic Optical Fiber Sensor for inSitu Monitoring of Scale-Forming Salts, Industrial & Engineering Chemistry Research, **47** (2008), no. 4, pp. 1066-1070.
89. Zibaii, M. I.; Kazemi, A.; Latifi, H.; Azar, M. K.; Hosseini, S. M. and Ghezelaiagh, M. H.: Measuring bacterial growth by refractive index tapered fiber optic biosensor, Journal of photochemistry and photobiology. B, Biology, **101** (2010), no. 3, pp. 313-320.
90. Ziemann, O.; Krauser, J.; Zamzow, P. E. and Daum, W.: POF-Handbuch: Optische Kurzstrecken-Übertragungssysteme, 2nd ed., Springer, Dordrecht, 2007.
91. Gaffey, S. J.: Spectral reflectance of carbonate minerals in the visible and near infrared (0.35 – 2.55 μm): Anhydrous carbonate minerals, Journal of Geophysical Research, **92** (1987), B2, p. 1429.

Received 7 July 2021, accepted 1 September 2021